

General Framework of Bound States in the Continuum in an Open Acoustic Resonator

Lujun Huang,^{1,*,**} Bin Jia,^{2,***} Artem S. Pilipchuk,^{3,***} Yankei Chiang,¹ Sibo Huang¹, Junfei Li¹,⁴ Chen Shen¹,⁵ Evgeny N. Bulgakov¹,³ Fu Deng,¹ David A. Powell¹, Steven A. Cummer,⁴ Yong Li¹,^{2,†} Almas F. Sadreev,^{3,‡} and Andrey E. Miroshnichenko^{1,§}

¹ School of Engineering and Information Technology, University of New South Wales, Northcott Drive, Canberra, ACT 2600, Australia

² Institute of Acoustics, Tongji University, Shanghai 200092, People's Republic of China

³ L. V. Kirensky Institute of Physics, Federal Research Center KSC Siberian Branch, RAN, Krasnoyarsk 660036, Russia

⁴ Department of Electrical and Computer Engineering, Duke University, Durham, North Carolina 27708, USA

⁵ Department of Mechanical Engineering, Rowan University, Glassboro, New Jersey 08028, USA



(Received 6 August 2022; revised 14 September 2022; accepted 20 October 2022; published 8 November 2022)

Bound states in the continuum (BICs) provide a viable way of achieving high- Q resonances in both photonics and acoustics. In this work, we propose a general method of constructing Friedrich-Wintgen (FW) BICs and accidental BICs in a coupled acoustic waveguide-resonator system. We demonstrate that FW BICs can be achieved with arbitrary two degenerate resonances in a closed resonator, regardless of whether they have the same or opposite parity. Moreover, their eigenmode profiles can be arbitrarily engineered by adjusting the position of the attached waveguide. This suggests an effective way of continuously switching the nature of the BICs from FW BICs to symmetry-protected BICs or accidental BICs. Also, such BICs are sustained in the coupled waveguide-resonator system with shapes such as rectangles, ellipses, and rhomboids. These interesting phenomena are well explained by the two-level effective non-Hermitian Hamiltonian, where two strongly coupled degenerate modes play a major role in forming such FW BICs. Additionally, we find that such an open system also supports accidental BICs in geometry space instead of momentum space via tuning the position of the attached waveguide, which is attributed to the quenched coupling between the waveguide and eigenmodes of the closed cavity. Finally, we fabricate a series of three-dimensional coupled resonator waveguides and experimentally verify the existence of FW BICs and accidental BICs by measuring the transmission spectra. Our results complement the current BIC library in acoustics and provide nice routes for designing acoustic devices, such as acoustic absorbers, filters, and sensors.

DOI: 10.1103/PhysRevApplied.18.054021

I. INTRODUCTION

Bound states in the continuum (BICs) have attracted broad interest across the photonic community in the past 10 years due to their extraordinary optical properties [1,2]. They correspond to trapped modes, despite being localized within the continuous spectrum, thus having an infinitely large Q factor. Usually, BICs must be converted into quasi-BICs (QBICs) with finite high- Q factors for

practical application because only QBICs can be accessed by external excitation. The most salient property of BICs is that they suggest a viable way of realizing ultrahigh- Q resonances, whereas extreme field confinement is enabled for boosting light-matter interactions [3–6]. Different types of BICs or QBICs, including symmetry-protected (SP) BICs [7–10], accidental BICs [8,11], Friedrich-Wintgen (FW) BICs [12–16], and Fabry-Perot BICs [17–21], are demonstrated in an array structure of nanoparticles or a photonic waveguide system.

In recent years, increasing attention has been paid to acoustic BICs, also called trapped modes. SP BICs have been intensively studied by different groups [22–26]. For example, Evans and Porter considered SP BICs in a directional two-dimensional waveguide with a symmetrically loaded rigid circular obstacle [22]. Hein *et al.* found that

*ljhuang@mail.sitp.ac.cn

†yongli@tongji.edu.cn

‡almas@tnp.krasn.ru

§andrey.miroshnichenko@unsw.edu.au

**L. Huang, B. Jia, and A. S. Pilipchuk contributed equally to this work.

placing an object in a duct could excite a quasi-trapped mode if symmetry was broken, leading to a high- Q Fano resonance [25]. Fabry-Perot BICs have been numerically studied by Hein *et al.* [27]. They found that Fabry-Perot BICs happened only when two resonators were separated by certain distances. FW BICs, known as embedded trapped modes, have been theoretically studied by Hein *et al.* [27], Lyapina *et al.* [28,29], and Dai [30].

Some early attempts at the experimental verification of SP BICs were conducted by Parker [31,32] and Cobelli *et al.* [33]. Recently developed three-dimensional (3D) printing technology enables researchers to verify these BICs. Huang *et al.* experimentally demonstrated the existence of SP BICs, FW BICs, and mirror-induced BICs [34]. Soon after, the same group demonstrated topological BICs [35] that arose from the merging of two Fabry-Perot BICs. Since the Q factor of QBICs can be flexibly tuned by structural parameters, they are used to realize perfect absorption for both acoustic waves [36] and elastic waves [37]. Although significant progress has been made in the past few years, some open questions still remain unanswered. (1) Is it possible to construct a FW BIC based on any two degenerate resonances, regardless of whether or not their parities are the same? FW BICs are found in both photonics and acoustics [13–15,28,34]. However, the two resonances must have the same parity and cross each other at certain geometric parameters, such that their field profiles interchange with each other. (2) Can the eigenfield profile of FW BICs be arbitrarily engineered? Can the nature of BICs be switched from one type to another? (3) Do accidental BICs exist in a finite system? Accidental BICs are found at the off- Γ point in the first Brillouin zone in a photonic crystal slab [11]. However, the first Brillouin cannot be defined in such a finite system.

Here, we report a general framework of BICs in an open acoustic system. We find that FW BICs can be constructed by any two degenerate resonances in a closed resonator, regardless of whether these two resonances have the same or opposite parity. Furthermore, tuning the waveguide position allows one to control the FW BIC's eigenfield profile arbitrarily, allowing for a continuous transition from a FW BIC to a SP BIC (or an accidental BIC). Additionally, we find that such open systems support accidental BICs in geometric space by tuning the position of the attached waveguide. The formation mechanisms of both FW BICs and accidental BICs are explained by the effective non-Hermitian two-level Hamiltonian. Finally, we experimentally demonstrate the existence of FW BICs and accidental BICs by fabricating a series of 3D coupled resonator-waveguide systems and measuring their transmission spectra. The BICs are manifested by the vanishing linewidth resulting from collapse of the Fano resonance [38]. The Q factor retrieved from the transmission spectrum is up to 340. Our findings on these BICs may

find intriguing applications in realizing high-performance acoustic devices, such as filters and sensors.

II. RESULTS AND DISCUSSION

A. General Friedrich-Wintgen BICs

We start by investigating the resonant modes in three types of coupled waveguide-resonator systems: a single-port waveguide-resonator system [Figs. 1(a)–1(c)] and two-port waveguide-resonator systems with odd [Figs. 1(d)–1(f)] and even [Figs. 1(g)–1(i)] symmetry. For the sake of simplicity, we focus on the two-dimensional (2D) coupled waveguide-resonator systems to illustrate all possible BICs in these three systems comprehensively. Notably, under certain circumstances, BICs supported in Fig. 1(c) are equivalent to BICs in Figs. 1(f) and 1(i), which is proved in Sec. II C. Thus, we first consider the BICs in a single-port waveguide-resonator system, as shown in Fig. 1(c). The exterior boundary of the waveguide and resonator are set as a hard boundary to mimic acoustic wave propagation in the real acoustic system. Without loss of generality, we set the width of the two waveguides as $d = 10$ cm and the height of the rectangular resonator as $L_y = 20$ cm. Also, we define the size ratio of the resonator as $R = L_y/L_x$, where L_x is the width of the rectangular resonator. In our previous study [34], we demonstrated that such an open non-Hermitian system supported a series of leaky modes, usually denoted as M_{ml} (m and l are the number of antinodes along the x and y axes, respectively). Each leaky mode is represented by a complex eigenfrequency, $\omega = \omega_0 - i\gamma$, with its Q factor, $Q = \omega_0/2\gamma$, where ω_0 and γ are, respectively, the resonant frequency and radiative decay rate. Importantly, the leaky modes supported by this open system play a dominant role in controlling the reflection (transmission) spectra, as demonstrated by temporal coupled-mode theory [34,39]. Thus, searching for BICs turns to finding leaky modes with a zero radiative-decay rate or an infinite Q factor. Here, the leaky modes are calculated by using the commercial software package COMSOL Multiphysics.

Remarkably, we find that the structure shown in Fig. 1(c) supports many types of BICs. Figure 2(a) shows the BIC with the lowest eigenfrequency, the eigenfield distribution of which is displayed in the inset when R is varied from 0.95 to 1. Interestingly, this BIC also exists in the two-port system with odd symmetry, as shown in Fig. 2(b). Careful examination on the eigenfield profile suggests that such a BIC is the superposition of the eigenfield profiles of modes M_{12} and M_{21} of a closed cavity [see Fig. 2(c)], which can be fitted as

$$\psi_{\text{BIC}}(x, y) \approx A\psi_{21}(x, y) + B\psi_{12}(x, y), \quad (1)$$

where ψ_{12} and ψ_{21} represent the eigenfield distributions of closed-cavity modes M_{12} and M_{21} , respectively. A and B

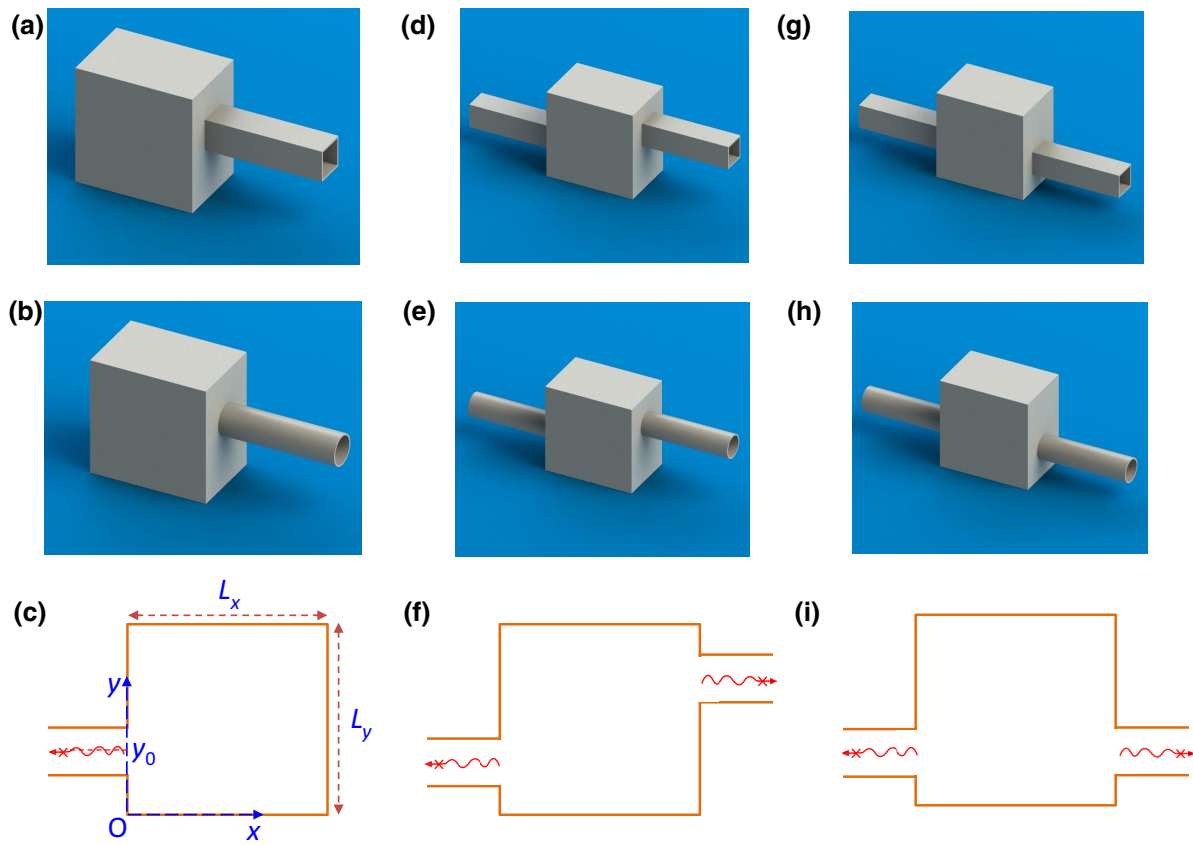


FIG. 1. Schematic drawing of an open resonator system. (a)–(c) Schematic illustration of a 3D single-port waveguide-resonator system with square or circular cross sections and its 2D equivalent. (d)–(f) Schematic illustration of a 3D two-port waveguide resonator system with odd symmetry and its 2D equivalent. (g)–(i) Schematic illustration of a 3D two-port waveguide-resonator system with even symmetry and its 2D equivalent.

are found to be 0.411 and -0.912 , respectively. We show how to derive the coefficients in Sec. II C 1. The lowest eigenmodes, M_{21} and M_{12} , are chosen because they belong to different irreducible representations of group-symmetry $C_{2\sigma}$. All of the leaky modes in the open rectangular resonator can be decomposed into the eigenmodes in the closed system, which form the complete orthogonal basis. It is necessary to point out that such a BIC has never been observed before, in either photonics or acoustics. Since the right and bottom hard boundaries can be viewed as two partial mirrors, this FW BIC corresponds to the FW BICs in a extended resonator sandwiched between two acoustic waveguides, as shown in Fig. 2(d). The BIC's eigenfield profile is equivalent to one quarter of the eigenfield profile of Friedrich-Wintgen BIC M_{13} [see the inset of Fig. 2(d)]. More examples can be easily constructed by finding the FW BICs in a two-port waveguide–full-resonator system [see Figs. 2(e) and S1 within the Supplemental Material [47]]. In Sec. II C 1, we demonstrate that these BICs are FW BICs. For example, the BICs in Figs. 2(a) and 2(b) are the result of destructive interference of eigenmodes M_{12} and M_{21} in a closed cavity, although these two modes have

opposite parity. A similar situation also occurs for the BIC in Fig. 2(e), which is attributed to the destructive interference of modes M_{31} and M_{22} in the closed cavity. Here, it is worth commenting that the mirror-induced BICs shown in Fig. 2(g) in Ref. [34] also belong to FW BICs. They are caused by the destructive interference of eigenmodes M_{21} and M_{13} in a closed resonator (Fig. S2 within the Supplemental Material [47]). In addition, it is worth pointing out that a rectangular resonator is not the only resonator that can host such BICs. We also find this BIC in an elliptical resonator [Fig. 2(f)] and a rhomboid resonator system (Fig. S3 within the Supplemental Material [47]).

Note that such a FW BIC always exists, even when the attached waveguide position is moved along four sides [Fig. S4(a) within the Supplemental Material [47]]. Interestingly, its eigenfield profile can be arbitrarily engineered by adjusting the position of the attached waveguide, which is manifested in Fig. 3(a). Moreover, it is found that this FW BIC can be switched to a SP BIC when the attached waveguide position is moved from the bottom to the middle point. Any other intermediate state can be viewed as the superposition of two eigenmodes, M_{12} and M_{21} , of a

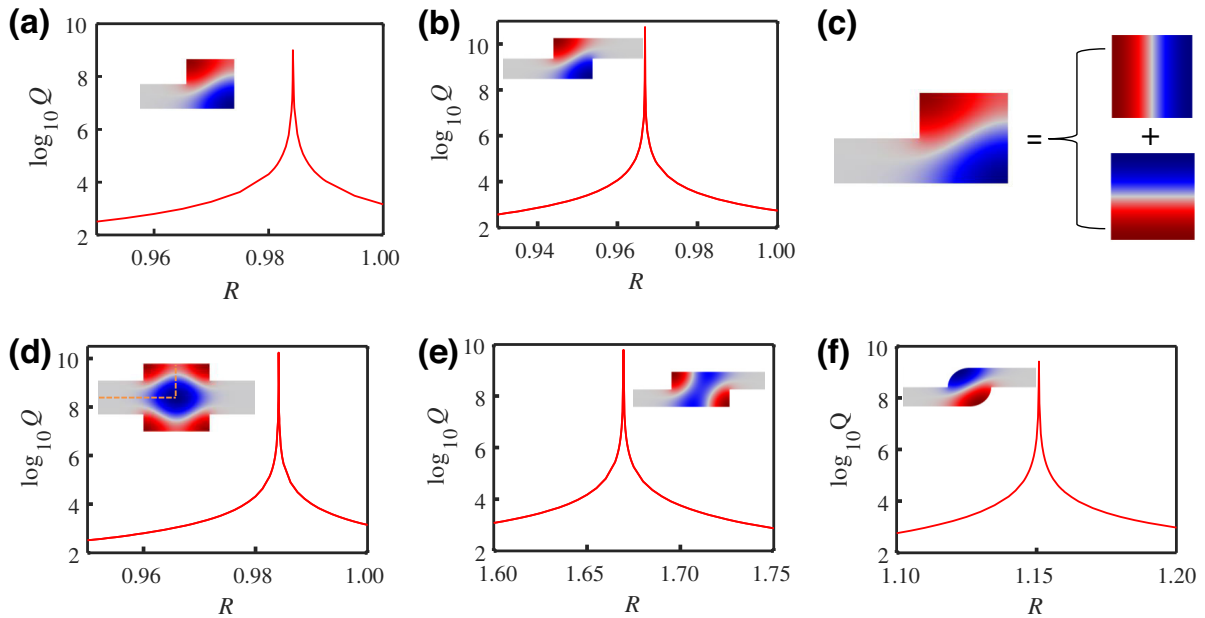


FIG. 2. FW BICs in an open resonator. (a) Q factor of a FW BIC in a single-port system versus the size ratio, R . Inset shows the eigenfield profile of the BIC. (b) Q factor of a FW BIC in a two-port system with odd symmetry versus the size ratio, R . Inset shows the eigenfield profile of the BIC. (c) Decomposition of a FW BIC into closed-cavity modes M_{12} and M_{21} . (d) Q factor of a FW BIC in a coupled-waveguide–full-resonator system versus size ratio. (e) Q factor of another FW BIC in a two-port waveguide-resonator system with odd symmetry versus size ratio. (f) Q factor of a FW BIC in an open elliptical resonator versus size ratio.

closed cavity, which can be explicitly written as

$$\psi_{\text{BIC}}(x, y) \approx \cos \theta \psi_{21}(x, y) + \sin \theta \psi_{12}(x, y). \quad (2)$$

Therefore, one can speculate that the waveguide position rotates the BIC in the Hilbert space of the eigenmodes of the closed resonator by the angle θ . Figure 3 shows the particular case of this mapping. Importantly, similar phenomena also occur for other FW BICs, such as the one shown in Fig. 2(e) [Figs. S4(b) and S5 within the Supplemental Material [47]] and the one arising from destructive interference of closed-cavity modes M_{13} and M_{31} [Figs. S4(c) and S6 within the Supplemental Material [47]]. More examples are included in Figs. S7–S9 within the Supplemental Material [47]. Thus, we can safely conclude that FW BICs always exist in the systems shown in Figs. 1(c) and 1(f), and their eigenfields can be arbitrarily synthesized via tuning the position of the attached waveguide. Also, the nature of BICs can be switched from FW BICs to SP BICs at $\theta = \pi/2$.

B. General accidental BICs

Accidental BICs were reported in a photonic crystal slab by Hsu *et al.* [11]. They occur in the first Brillouin zone, located either along the x and y axes in momentum space or in four quadrants, depending on the structural parameters. However, it is difficult to define accidental BICs in a finite system using a similar strategy because one cannot define the first Brillouin zone in momentum space.

For the open resonator shown in Fig. 2, the accidental BIC can be defined as the eigenmode of a closed resonator, the coupling of which with the propagating mode of the waveguide accidentally turns to zero upon moving the waveguide [40]. Since accidental BICs in a periodic structure are found at the off- Γ point, while SP BICs are hosted at the Γ point, we may call BICs accidental BICs in Hilbert space [40] when the attached waveguide deviates from the middle point that usually hosts SP BICs like M_{12} and M_{22} . To illustrate this notion, we again consider the single-port waveguide-resonator system. Here, the width of the waveguide is still set as $d = 10$ cm. The width and height of the rectangular resonator are $L_x = 40$ cm and $L_y = 60$ cm, respectively. We have to point out here that the height and width of the resonator can take any other values, as long as the resonant frequencies of the target mode are below the cutoff frequency of the waveguide. Figure 4(a) shows the Q factor of mode M_{13} as the center of the waveguide shifts from 5 to 55 cm. Surprisingly, two BICs occur at $yc_1 = 15.45$ cm and $yc_2 = 44.55$ cm. Figure 4(b) shows the eigenfield distribution of two BICs. Note that these two BICs are not independent of each other. They follow $yc_1 + yc_2 = L_y$. This is because mode M_{13} is symmetric with respect to $yc = 30$ cm. If there is a BIC at yc_0 , another BIC appears at $yc = L_y - yc_0$. Such BIC pairs are also found in a two-port waveguide-resonator system with even or odd symmetry, as confirmed in Figs. 4(c)–4(f). Another common feature of these accidental BICs is that all critical positions are around $yc_1 = 15$ cm and $yc_2 = 45$ cm, which

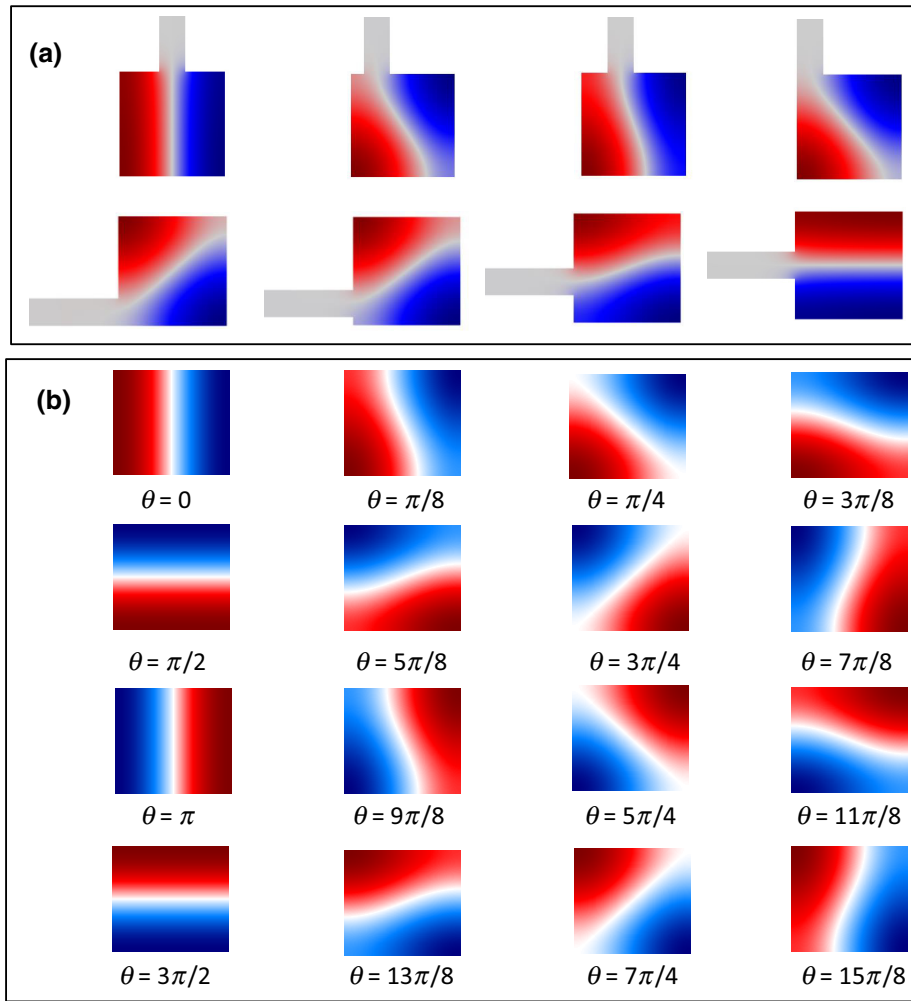


FIG. 3. Eigenfield-profile engineering of a FW BIC. (a) Eigenfield profile of a FW BIC for a single-port system with different attached waveguide positions. (b) Synthetic eigenfield profile based on modes M_{12} and M_{21} in a closed square resonator.

correspond to the nodes of closed-cavity mode M_{13} . Similarly, one could construct such accidental BICs based on modes M_{14} and M_{23} by altering the attached waveguide position (Fig. S10 within the Supplemental Material [47]).

C. Formation mechanism of these two BICs

To account for the formation of these BICs, we apply the method of an effective non-Hermitian Hamiltonian [2,41–45]. The Hamiltonian is the result of the Feshbach projection of total space onto the inner Hilbert space of eigenmodes in a closed resonator:

$$H_{\text{eff}} = H_R - \sum_{p=1}^{\infty} \sum_C i k_p W_{Cp} W_{Cp}^+, \quad (3)$$

where the first term, H_R , represents the dynamics of the closed resonator, and the matrices, W_{Cp} , represent the coupling of resonators modes with the p th channels of C th waveguides with wave number k_p .

Again, we consider the coupled waveguide-resonator system shown in Fig. 1(c). To make the conclusion as general as possible, we set the width of the waveguide as

$d = 1$ (unitless), and the width and height of the resonator are L_x and L_y , respectively. Also, for the sake of convenience, we take the bottom-left corner of the resonator as the origin, and the middle point of the attached waveguide position is $y = y_0$. Thus, the waveguide spans from $y = y_0 - 1/2$ to $y = y_0 + 1/2$. The first step is to compute the eigenfrequencies and eigenmodes of a closed resonator. They can be solved analytically with Neuman boundary conditions as follows:

$$\frac{v_{mn}^2}{\omega_0^2} = \frac{(m-1)^2}{L_x^2} + \frac{(n-1)^2}{L_y^2}, \quad (4a)$$

$$\psi_{mn}(x, y) = \sqrt{\frac{(2 - \delta_{m,1})(2 - \delta_{n,1})}{L_x L_y}} \cos\left[\frac{\pi(m-1)x}{L_x}\right] \times \cos\left[\frac{\pi(n-1)y}{L_y}\right], \quad (4b)$$

where v_{mn} is the resonant frequency and $\omega_0 = \pi v/d = \pi v$; v is the velocity of sound in air.

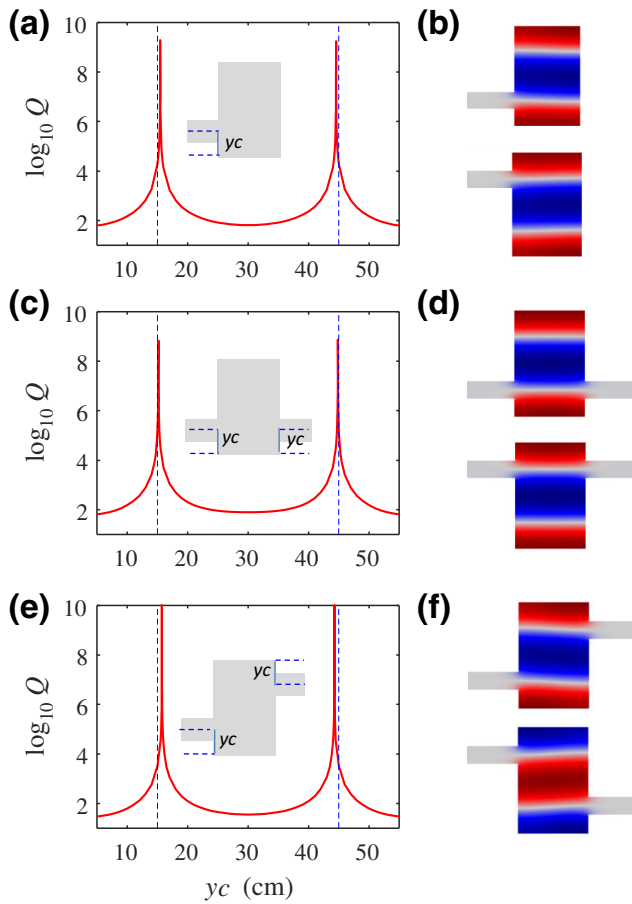


FIG. 4. Accidental BICs in an open resonator. (a) Q factor of accidental BICs in a single-port system with an attached waveguide located at different positions, y_c . (b) Eigenfield profile of two accidental BICs in a single-port system. (c) Q factor of accidental BICs in a two-port system with even symmetry. (d) Eigenfield profile of two accidental BICs in a two-port system with even symmetry. (e) Q factor of accidental BICs in a two-port system with odd symmetry. (f) Eigenfield profile of two accidental BICs in a two-port system with odd symmetry. All three resonators have dimensions $L_x = 40$ cm and $L_y = 60$ cm.

The propagating wave numbers in the waveguide are given by

$$\frac{v^2}{\omega_0^2} = \frac{k_p^2}{\pi^2} + (p - 1)^2, \quad (5a)$$

$$\phi_p(x, y) = \sqrt{(2 - \delta_{p,1})} \cos[\pi(p - 1)y] e^{ik_p x}. \quad (5b)$$

Then the coupling matrix elements between eigenmodes of the closed resonator and the p th propagation channels of the waveguide can be obtained by

$$W_{mn,p} = \int_{y_0-(1/2)}^{y_0+(1/2)} \psi_{m,n}(x = 0, y) \phi_p(x = 0, y) dy. \quad (6)$$

After obtaining the coupling matrix, we calculate the complex eigenvalues of the effective Hamiltonian, the real parts of which correspond to the resonant frequencies, and the imaginary parts are half of the resonant linewidth. Thus, searching for BICs amounts to finding the zero imaginary part of the eigenvalues. In general, the eigenfunction of each BIC can be decomposed as

$$\phi_{\text{BIC}}(x, y) = \sum_{mn} a_{mn} \psi_{mn}(x, y). \quad (7)$$

Since the BIC is perfectly decoupled from the continuum, its eigenfunction must follow

$$\int_{y_0-(1/2)}^{y_0+(1/2)} \phi_{\text{BIC}}(x = 0, y) dy = 0. \quad (8)$$

1. Physical mechanism of FW BICs

When two resonant states approach each other as a function of a certain continuous parameter, interference causes an avoided crossing of the two states in their energy positions. Simultaneously, one of the resonant linewidths vanishes exactly at a certain value of the parameters and the other is boosted to maximum. These are known as FW BICs [12]. They are found in a single dielectric [13,14] and acoustic [28,34] resonator with a rectangular cross section. However, when constructing such FW BICs, two resonances must have the same parity and cross each other at a certain size ratio for the closed cavity. Thus, a pair of eigenmodes, M_{mn} and $M_{m+2,n-2}$ (or M_{mn} and $M_{m-2,n+2}$), are frequently used for building FW BICs because they satisfy both requirements. Also, the eigenfield profile may interchange with each other when the size ratio of the rectangular resonator passes through the critical value.

Since the essence of finding FW BICs is to find two degenerate resonances in a closed resonator at a certain size ratio, in principle, there should be numerous choices of paired modes not limited to modes M_{mn} and $M_{m+2,n-2}$. In the present paper, we consider the FW BIC in a rectangular resonator embedded into the first channel, $p = 1$, provided that other channels are closed for $v < 1$. There are numerous degeneracies in a closed rectangular resonator:

$$\frac{m^2}{L_x^2} + \frac{n^2}{L_y^2} = \frac{m'^2}{L_x^2} + \frac{n'^2}{L_y^2}. \quad (9)$$

The lowest case corresponds to $m, n = 1, 2$ and $m', n' = 2, 1$ for a square resonator, $L_x = L_y$. The other degeneracies happening in a square resonator satisfy $m = n'$ and $n = m'$. The second-lowest degeneracy in a rectangular resonator is $m, n = 2, 2$ and $m', n' = 3, 1$ for $L_x = \sqrt{3}L_y$. All of these degeneracies can be used to construct FW BICs in the single-port waveguide-resonator system or two-port waveguide-resonator system with odd symmetry.

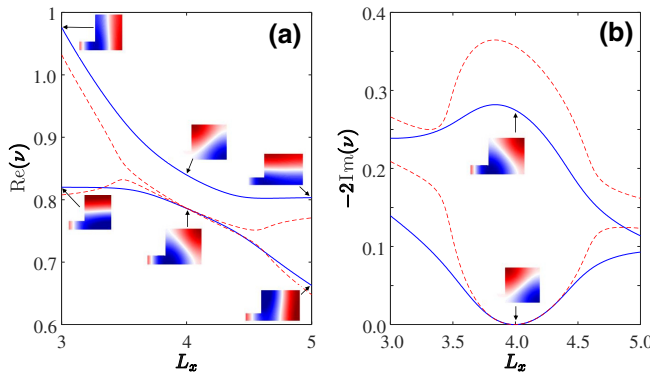


FIG. 5. Formation mechanism of FW BICs. Real part (a) and imaginary part (b) of eigenfrequency in a single-port system when 20 eigenstates are considered for calculating the complex eigenfrequencies (solid blue line). Dashed line corresponds to the case where only closed-cavity modes M_{12} and M_{21} are considered.

Figure 5 shows the behavior of real and imaginary parts of complex eigenvalues for two resonances in the effective Hamiltonian. The solid line represents the results for the effective Hamiltonian, considering 20 eigenstates in the closed resonator, and the dashed line corresponds to the case of the effective Hamiltonian, which involves only eigenmodes M_{12} and M_{21} of the closed resonator. From Fig. 5, we indeed observe the avoided crossing at $L_x = 3.9942$, around which one of the imaginary parts is suppressed to zero, and the other is boosted to maximum. These match the features of FW BICs. Interestingly, the formation of such a BIC can be mainly attributed to the destructive interference of modes M_{12} and M_{21} in a closed resonator, as demonstrated by the dashed line of Figs. 5(a) and 5(b). Thus, we may approximate the eigenfunction of the lowest-order FW BIC as a superposition of the two eigenmodes of the closed resonator, and their coefficients A and B can be rigorously calculated by

$$\psi_{\text{BIC}}(x, y) \approx A\psi_{21}(x, y) + B\psi_{12}(x, y). \quad (10)$$

Substituting Eq. (10) into Eq. (8) gives us

$$A = W_{12;p=1} = \frac{1}{\pi} \sqrt{\frac{2L_y}{L_x}} \left[\sin \frac{\pi}{L_y} \left(y_0 + \frac{1}{2} \right) - \sin \frac{\pi}{L_y} \left(y_0 - \frac{1}{2} \right) \right], \quad (11a)$$

$$B = -W_{21;p=1} = -\sqrt{\frac{2}{L_x L_y}}. \quad (11b)$$

Excellent agreement is found between the eigenfield profile predicted from Eqs. (10) and (11) and the numerically calculated eigenfield profile of the FW BIC (Fig. S11 within the Supplemental Material [47]) when y_0 varies

from 0.5 to 2. Another interesting point is that such a FW BIC is reduced to a SP BIC at $y_0 = L_y/2$ due to $W_{12;p=1} = 0$. Although modes M_{12} and M_{21} in the closed resonator play a major role in the formation of a FW BIC, the coupling between the evanescent modes of the waveguide with imaginary k_p ($p = 2, 3, \dots$) and eigenmodes in the closed resonator leads to a slight deviation of L_y from $L_y = 4$. Following a similar strategy, we can construct more FW BICs by finding resonance degeneracies based on Eq. (7). Their formation can also be explained by destructive interference between two major resonant modes. For example, the FW BIC shown in Fig. 2(e) is the result of coupling between modes M_{22} and M_{31} (Fig. S12 within the Supplemental Material [47]). The synthetic eigenfield profile of such a FW BIC is also confirmed using this analytical model (Fig. S13 within the Supplemental Material [47]). Excellent agreement is also found for mirror-induced BICs (Fig. S14 within the Supplemental Material [47]).

2. Physical mechanism of accidental BICs and SP BICs

When only the first channel, $p = 1$, is considered for $\nu < 1$, the key to realizing BICs is to find $W_{mn;p=1} = 0$. It is easy to find that zero coupling between the waveguide and mode M_{mn} happens at

$$y_0 = \frac{2s+1}{2(n-1)} L_y, \quad s = 1, 2, \dots, n-1. \quad (12)$$

Equation (12) predicts the critical waveguide positions around which BICs can be found in a real system. Note that accidental BICs can be found only for $n > 2$. When n is even, both accidental BICs and SP BICs are supported in such a system. In Fig. 4, dashed vertical lines indicate the predicted y_{C0} with $W_{mn;p=1} = 0$, which is very close to the observed value y_C of the BICs. The slight difference between them is ascribed to the fact that there is a small contribution from higher eigenmodes M_{22} and M_{23} owing to evanescent modes with $p = 2$ (see Sec. S1 and Fig. S15 within the Supplemental Material [47]). Here, it is necessary to highlight the difference between accidental BICs and SP BICs, although the attached waveguide is almost located at the nodal line of the eigenfield profile of BICs. Due to coupling of the eigenmodes to evanescent modes of the waveguide, the critical position of the attached waveguide slightly deviates from the nodal line of the eigenfield in the closed resonator. However, for SP BICs, the waveguide is attached at the exact position of the nodal line of the eigenfield in the closed resonator due to the compatibility of structural symmetry. Additionally, the whole structure no longer preserves its symmetry for the structure supporting accidental BICs. This is the reason why we define these BICs as accidental BICs.

3. Symmetry considerations

As shown in Sec. II A, the system shown in Fig. 1(f) can support similar FW BICs to those shown in Fig. 1(c). For a two-port systems with even or odd symmetry, it is easy to derive

$$W_{mn;p=1}^L = (-1)^{m-1} W_{mn;p=1}^R, \quad (13a)$$

$$W_{mn;p=1}^L = (-1)^{m+n} W_{mn;p=1}^R. \quad (13b)$$

Thus, if FW BICs are sustained in a single-port waveguide-resonator system, from Eq. (13b) one can immediately find such FW BICs in a two-port waveguide-resonator system with odd symmetry. We use the FW BIC shown in Fig. 2(a) as an example to illustrate this notion; it has $C_1 W_{12;p=1}^L + C_2 W_{21;p=1}^L = 0$. According to Eq. (13b), odd symmetry of the structure requires $C_1 W_{12;p=1}^R + C_2 W_{21;p=1}^R = -C_1 W_{12;p=1}^L - C_2 W_{21;p=1}^L = 0$. Equation (13) also explains why the lowest-order FW BIC in a square resonator is M_{13} when the left and right waveguides are located at the middle point of the left and right sides. Additionally, Eq. (13a) explains how two-port systems with either even or odd symmetry support accidental BICs like a single-port system.

D. Experimental verification of general FW BICs and accidental BICs

We would like to emphasize that such FW BICs and accidental BICs also exist in the 3D case. For experimental consideration, we study a 3D resonator coupled to two shifted cylindrical waveguides, as shown in Fig. 6(a). The diameter of the cylindrical waveguide is set as $D = 29$ mm. The resonator has dimensions $L_x = 2D = 58$ mm, $L_y = 29$ mm. By sweeping L_z from 49.7 to 52.2 mm, we find that there is a BIC at $L_z = 50.89$ mm, as confirmed in the top panel of Fig. 6(b). Its eigenfield distribution is shown in the right panel of Fig. 6(a), similar to the eigenfield profile of the 2D case shown in Fig. 2(b). The emergence of the BIC is also confirmed by calculating the transmission-spectra mapping shown in the top panel of Fig. 6(c), which indeed shows a vanishing linewidth at $L_z = 50.89$ mm. Then, we move to demonstrate the existence of such a BIC experimentally. We fabricate a series of samples with different L_z , covering the range from 49.7 to 52.2 mm. The bottom panel of Fig. 6(c) shows the measured transmission-spectra mapping. Excellent agreement is found between experiment and simulation. By applying a Fano-resonance fitting procedure [39,46] (see Sec. S2 and Fig. S16 within the Supplemental Material [47]), we retrieve the Q factor of the acoustic resonance at different L_z . The relevant result is plotted in the bottom-left panel

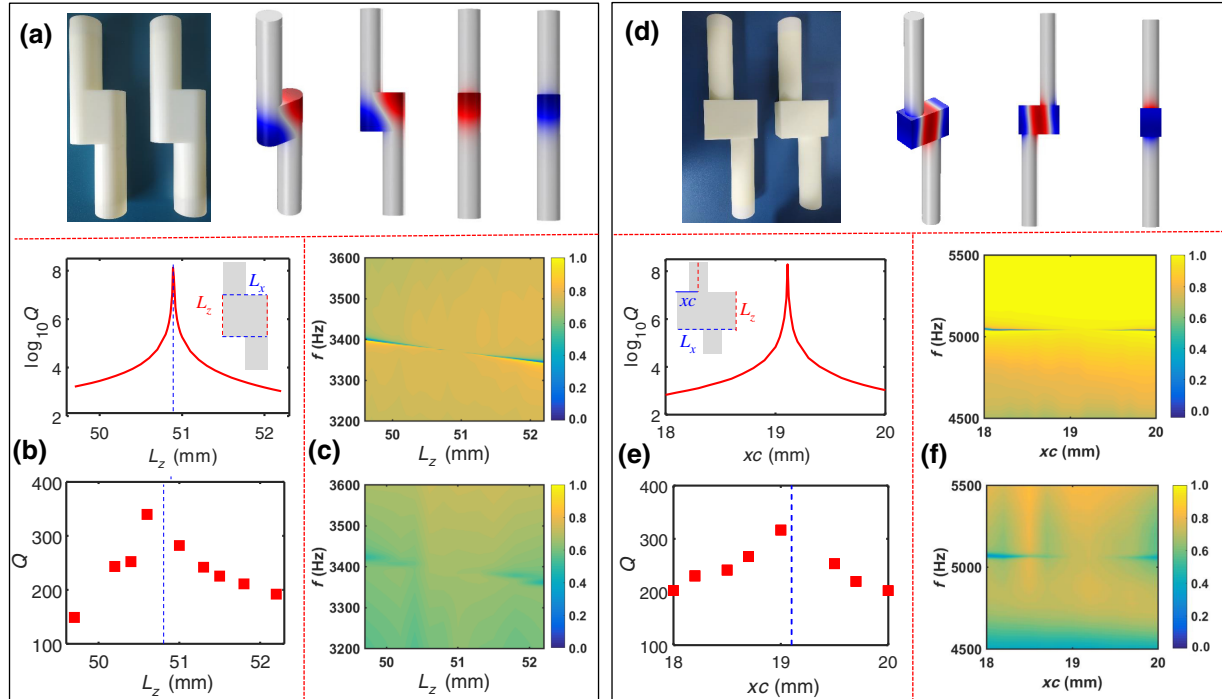


FIG. 6. Experimental demonstration of a FW BIC and an accidental BIC in a 3D open resonator with odd symmetry. (a) Left panel is the optical image of the 3D-printed sample, and right panel represents the eigenfield profile of a FW BIC. (b) Calculated and measured Q factor versus L_z . (c) Calculated and measured transmission-spectra mapping for L_z varying from 49.7 to 52.2 mm. (d) Left panel is the optical image of the 3D-printed sample, and right panel represents the eigenfield profile of an accidental BIC. (e) Calculated and measured Q factor versus xc . (f) Calculated and measured transmission-spectra mapping for xc varying from 18 to 20 mm.

of Fig. 6(b). The vertical dashed line indicates L_z showing the vanishing linewidth of resonance, indicating the formation of the BIC. The experimentally measured Q factor shows several orders of magnitude reduction compared to the theoretical prediction because of viscous losses in the real system. However, we still observe a relatively high- Q resonance with a Q factor up to 340, which is large enough for real applications. Additionally, we emphasize that this is not the only structure supporting such a FW BIC. More examples can be found in Fig. S17 within the Supplemental Material [47].

We also demonstrate the accidental BICs in such a two-port system. Figure 6(d) shows the optical image of a 3D-printed sample. The diameters of the two waveguides are also $D = 29$ mm. The dimensions of the cuboid resonator are $L_x = 70$ mm, $L_y = 36$ mm, and $L_z = 50$ mm. By varying the attached waveguide position, we find an accidental BIC at $x_c = 19.11$ mm, as seen in the top panel of Fig. 6(e). This critical position deviates slightly from $x_{c0} = L_x/4 = 17.5$ mm predicted by Eq. (11) because of the coupling between the evanescent modes in the waveguide and eigenmodes in the closed resonator. The existence of such a BIC is confirmed by the calculated transmission-spectra mapping shown in the top panel of Fig. 6(f). We fabricate nine samples using 3D-printing technology (see Sec. IV for details). Excellent agreement can be found between the measured transmission spectra [bottom panel of Fig. 6(f)] and simulated transmission spectra. We also retrieve their Q factors by Fano fitting and plot them in the bottom panel of Fig. 6(e). The overall trend in Q factor matches reasonably well with the calculated Q factor, although the measured one is several orders lower than the numerical prediction due to the viscous losses inside the waveguide and resonator. However, all Q factors are above 200, which is large enough for many applications. Also, we find further examples of accidental BICs in such a two-port waveguide–3D-resonator system (Fig. S18 in the Supplemental Material [47]).

III. CONCLUSION

We report a general procedure for finding FW BICs and accidental BICs in an open acoustic resonator. We demonstrate that FW BICs can be constructed by any two degenerate resonances with either the same or opposite parity in a single-port system or two-port system with odd symmetry. Moreover, their eigenfield profile can be arbitrarily synthesized by tuning the waveguide position, similar to the case of quantum mechanics. Also, FW BICs can be switched to either SP BICs or accidental BICs when the waveguide is placed at a certain position. In addition, we find that such an open system supports accidental BICs as the vector in Hilbert space of the eigenmodes of the closed resonator, the direction of which changes with the position of the attached waveguide that breaks

the symmetry of the closed resonator. The formation of both FW BICs and accidental BICs is well explained by the effective Hamiltonian method. The former is attributed to the destructive interference of two eigenmodes in the closed cavity, while the latter arises from the suppressed coupling between propagation modes in the waveguide and eigenmode in the closed resonator. Finally, we experimentally demonstrate both FW BICs and accidental BICs in a 3D coupled waveguide-resonator system with odd symmetry. The emergence of BICs is evidenced by the vanishing linewidth of the acoustic resonance. Our findings promise many exciting applications, such as enhanced acoustic emission, ultranarrowband acoustic absorbers, acoustic filters, and sensors.

IV. MATERIALS AND METHODS

A. Simulations

All simulations are performed with the commercial software package COMSOL Multiphysics. The speed of sound and density of air are 343 m/s and 1.29 kg/m³, respectively. When calculating the eigenmodes and transmission (or reflection spectrum), we apply perfectly matched layer boundaries at the two ends of the waveguides to mimic acoustic wave propagation in infinite space. The other exterior boundaries are set as rigid.

B. Experiments

The experimental samples are fabricated by using 3D-printing technology with laser sintering stereolithography (SLA, 140 μm) with a photosensitive resin (UV curable resin), exhibiting a manufacturing precision of 0.1 mm. The complex transmission (and reflection) coefficients of the samples are measured using a Brüel & Kjær type-4206T impedance tube with a diameter of 29 mm. A loudspeaker generates a plane wave, and the amplitude and phase of local pressure are measured by four 1/4-inch condenser microphones (Brüel & Kjær type-4187) situated at designated positions. The complex transmission (and reflection) coefficients are obtained by the transfer-matrix method.

ACKNOWLEDGMENTS

L.H. and A.E.M. are supported by the Australian Research Council Discovery Project (Grant No. DP200101353) and the UNSW Scientia Fellowship program. Y.K.C. and D.A.P. are supported by the Australian Research Council Discovery Project (Grant No. DP200101708). B.J., S.H., and Y.L. are supported by the National Natural Science Foundation of China (Grant No. 12074286) and the Shanghai Science and Technology Committee (Grant No. 21JC1405600). A.P., E.B., and A.S. are supported by the Russian Science Foundation (Grant No. 22-12-00070).

L. Huang and A. E. Miroshnichenko conceived the idea. L. Huang, A. S. Pilipchuk, and A. F. Sadreev performed the theoretical calculation and numerical simulation. B. Jia, S. Huang, and Y. Li fabricated the sample and performed the reflection and transmission spectra measurements. Y. K. Chiang, J. Li, C. Shen, E. N. Bulgakov, F. Deng, D. A. Powell, and S. Cummer helped with the numerical simulation. L. Huang, Y. Li, A. F. Sadreev, and A. E. Miroshnichenko supervised the project. All authors discussed the results and prepared the manuscript.

-
- [1] C. W. Hsu, B. Zhen, A. D. Stone, J. D. Joannopoulos, and M. Soljačić, Bound states in the continuum, *Nat. Rev. Mater.* **1**, 16048 (2016).
 - [2] A. F. Sadreev, Interference traps waves in an open system: Bound states in the continuum, *Rep. Prog. Phys.* **84**, 55901 (2021).
 - [3] A. Kodigala, T. Lepetit, Q. Gu, B. Bahari, Y. Fainman, and B. Kanté, Lasing action from photonic bound states in continuum, *Nature* **541**, 196 (2017).
 - [4] L. Xu, K. Z. Kamali, L. Huang, M. Rahmani, A. Smirnov, R. Camacho-Morales, Y. Ma, G. Zhang, M. Woolley, D. Neshev, A. E. Miroshnichenko, Dynamic nonlinear image tuning through magnetic dipole quasi-BIC ultrathin resonators, *Adv. Sci.* **6**, 1802119 (2019).
 - [5] I. Volkovskaya, L. Xu, L. Huang, A. I. Smirnov, A. E. Miroshnichenko, and D. Smirnova, Multipolar second-harmonic generation from high- Q quasi-BIC states in subwavelength resonators, *Nanophotonics* **9**, 3953 (2020).
 - [6] K. Koshelev, Y. Tang, K. Li, D.-Y. Choi, G. Li, and Y. Kivshar, Nonlinear metasurfaces governed by bound states in the continuum, *ACS Photonics* **6**, 1639 (2019).
 - [7] K. Koshelev, S. Lepeshov, M. Liu, A. Bogdanov, and Y. Kivshar, Asymmetric Metasurfaces with High- Q Resonances Governed by Bound States in the Continuum, *Phys. Rev. Lett.* **121**, 193903 (2018).
 - [8] E. N. Bulgakov and A. F. Sadreev, Bloch bound states in the radiation continuum in a periodic array of dielectric rods, *Phys. Rev. A* **90**, 53801 (2014).
 - [9] J. Lee, B. Zhen, S.-L. Chua, W. Qiu, J. D. Joannopoulos, M. Soljačić, and O. Shapira, Observation and Differentiation of Unique High- Q Optical Resonances Near Zero Wave Vector in Macroscopic Photonic Crystal Slabs, *Phys. Rev. Lett.* **109**, 67401 (2012).
 - [10] S. Li, C. Zhou, T. Liu, and S. Xiao, Symmetry-protected bound states in the continuum supported by all-dielectric metasurfaces, *Phys. Rev. A* **100**, 63803 (2019).
 - [11] C. W. Hsu, B. Zhen, J. Lee, S. L. Chua, S. G. Johnson, J. D. Joannopoulos, and M. Soljačić, Observation of trapped light within the radiation continuum, *Nature* **499**, 188 (2013).
 - [12] H. Friedrich and D. Wintgen, Interfering resonances and bound states in the continuum, *Phys. Rev. A* **32**, 3231 (1985).
 - [13] L. Huang, L. Xu, M. Rahmani, D. Neshev, and A. E. Miroshnichenko, Pushing the limit of high- Q mode of a single dielectric nanocavity, *Adv. Photonics* **3**, 016004 (2021).
 - [14] M. V. Rybin, K. L. Koshelev, Z. F. Sadrieva, K. B. Samusev, A. A. Bogdanov, M. F. Limonov, and Y. S. Kivshar, High- Q Supercavity Modes in Subwavelength Dielectric Resonators, *Phys. Rev. Lett.* **119**, 243901 (2017).
 - [15] A. F. Sadreev, E. N. Bulgakov, and I. Rotter, Bound states in the continuum in open quantum billiards with a variable shape, *Phys. Rev. B* **73**, 235342 (2006).
 - [16] T. Lepetit and B. Kanté, Controlling multipolar radiation with symmetries for electromagnetic bound states in the continuum, *Phys. Rev. B* **90**, 241103 (2014).
 - [17] Y. Sato, Y. Tanaka, J. Upham, Y. Takahashi, T. Asano, and S. Noda, Strong coupling between distant photonic nanocavities and its dynamic control, *Nat. Photonics* **6**, 56 (2012).
 - [18] W. Suh, M. F. Yanik, O. Solgaard, and S. Fan, Displacement-sensitive photonic crystal structures based on guided resonance in photonic crystal slabs, *Appl. Phys. Lett.* **82**, 1999 (2003).
 - [19] E. N. Bulgakov and A. F. Sadreev, Bound states in the continuum in photonic waveguides inspired by defects, *Phys. Rev. B* **78**, 75105 (2008).
 - [20] S. Weimann, Y. Xu, R. Keil, A. E. Miroshnichenko, A. Tünnermann, S. Nolte, A. A. Sukhorukov, A. Szameit, and Y. S. Kivshar, Compact Surface Fano States Embedded in the Continuum of Waveguide Arrays, *Phys. Rev. Lett.* **111**, 240403 (2013).
 - [21] D. C. Marinica, A. G. Borisov, and S. V. Shabanov, Bound States in the Continuum in Photonics, *Phys. Rev. Lett.* **100**, 1 (2008).
 - [22] D. Evans and R. Porter, Trapped modes embedded in the continuous spectrum, *Q. J. Mech. Appl. Math.* **51**, 263 (1998).
 - [23] C. M. Linton, M. McIver, P. McIver, K. Ratcliffe, and J. Zhang, Trapped modes for off-centre structures in guides, *Wave Motion* **36**, 67 (2002).
 - [24] S. Hein and W. Koch, Acoustic resonances and trapped modes in pipes and tunnels, *J. Fluid Mech.* **605**, 401 (2008).
 - [25] S. Hein, W. Koch, and L. Nannen, Fano resonances in acoustics, *J. Fluid Mech.* **664**, 238 (2010).
 - [26] Y. Duan, W. Koch, C. M. Linton, and M. McIver, Complex resonances and trapped modes in ducted domains, *J. Fluid Mech.* **571**, 119 (2007).
 - [27] S. Hein, W. Koch, and L. Nannen, Trapped modes and Fano resonances in two-dimensional acoustical duct-cavity systems, *J. Fluid Mech.* **692**, 257 (2012).
 - [28] A. A. Lyapina, D. N. Maksimov, A. S. Pilipchuk, and A. F. Sadreev, Bound states in the continuum in open acoustic resonators, *J. Fluid Mech.* **780**, 370 (2015).
 - [29] A. A. Lyapina, A. S. Pilipchuk, and A. F. Sadreev, Trapped modes in a non-axisymmetric cylindrical waveguide, *J. Sound Vib.* **421**, 48 (2018).
 - [30] X. Dai, Total reflection of two guided waves for embedded trapped modes, *AIAA J.* **59**, 131 (2020).
 - [31] R. Parker, Resonance effects in wake shedding from parallel plates: Some experimental observations, *J. Sound Vib.* **4**, 62 (1966).
 - [32] R. Parker, Resonance effects in wake shedding from parallel plates: Calculation of resonant frequencies, *J. Sound Vib.* **5**, 330 (1967).

- [33] P. J. Cobelli, V. Pagneux, A. Maurel, and P. Petitjeans, Experimental observation of trapped modes in a water wave channel, *Europhys. Lett.* **88**, 20006 (2009).
- [34] L. Huang, Y. K. Chiang, S. Huang, C. Shen, F. Deng, Y. Cheng, B. Jia, Y. Li, D. A. Powell, and A. E. Miroshnichenko, Sound trapping in an open resonator, *Nat. Commun.* **12**, 4819 (2021).
- [35] L. Huang, B. Jia, Y. K. Chiang, S. Huang, C. Shen, F. Deng, T. Yang, D. A. Powell, Y. Li, and A. E. Miroshnichenko, Topological supercavity resonances in the finite system, *Adv. Sci.* **9**, 2200257 (2022).
- [36] S. Huang, T. Liu, Z. Zhou, X. Wang, J. Zhu, and Y. Li, Extreme Sound Confinement from Quasibound States in the Continuum, *Phys. Rev. Appl.* **14**, 21001 (2020).
- [37] L. Cao, Y. Zhu, S. Wan, Y. Zeng, Y. Li, and B. Assouar, Perfect absorption of flexural waves induced by bound state in the continuum, *Extrem. Mech. Lett.* **47**, 101364 (2021).
- [38] C. S. Kim, A. M. Satanin, Y. S. Joe, and R. M. Cosby, Resonant tunneling in a quantum waveguide: Effect of a finite-size attractive impurity, *Phys. Rev. B* **60**, 10962 (1999).
- [39] S. Fan, W. Suh, and J. D. Joannopoulos, Temporal coupled-mode theory for the Fano resonance in optical resonators, *J. Opt. Soc. Am. A* **20**, 569 (2003).
- [40] A. S. Pilipchuk and A. F. Sadreev, Accidental bound states in the continuum in an open Sinai billiard, *Phys. Lett. A* **381**, 720 (2017).
- [41] H. Feshbach, Unified theory of nuclear reactions, *Ann. Phys.* **5**, 357 (1958).
- [42] F.-M. Dittes, The decay of quantum systems with a small number of open channels, *Phys. Rep.* **339**, 215 (2000).
- [43] J. Okołowicz, M. Płoszajczak, and I. Rotter, Dynamics of quantum systems embedded in a continuum, *Phys. Rep.* **374**, 271 (2003).
- [44] A. F. Sadreev and I. Rotter, *S*-Matrix theory for transmission through billiards in tight-binding approach, *J. Phys. A: Math. Gen.* **36**, 11413 (2003).
- [45] D. N. Maksimov, A. F. Sadreev, A. A. Lyapina, and A. S. Pilipchuk, Coupled mode theory for acoustic resonators, *Wave Motion* **56**, 52 (2015).
- [46] A. E. Miroshnichenko, S. Flach, and Y. S. Kivshar, Fano resonances in nanoscale structures, *Rev. Mod. Phys.* **82**, 2257 (2010).
- [47] See the Supplemental Material at <http://link.aps.org/supplemental/10.1103/PhysRevApplied.18.054021> for effect of evanescent mode in the waveguide to accidental BICs, fano resonance fitting, more examples of general FW-BICs and accidental BICs in an open acoustic resonator.